Effect of hadronic interaction on the flow of K^{*0}

Tribhuban Parida,* Sandeep Chatterjee,† and Md. Nasim‡
Department of Physical Sciences, Indian Institute of Science Education and Research Berhampur, Transit Campus (Govt ITI), Berhampur 760010, Odisha, India

(Received 3 January 2024; accepted 15 March 2024; published 8 April 2024)

We explore the implications of the late-stage hadronic rescattering phase on the flow of K^{*0}. The model calculations are done using a $(3+1)$-dimensional hybrid framework, incorporating both hydrodynamic evolution and hadronic transport that is calibrated to agree with bulk observables including the elusive rapidity differential v_1 of light-flavor hadrons. We find that the late-stage hadronic rescattering phase causes significant qualitative modification of the K^{*0} rapidity differential directed flow v_1 resulting in $\frac{dv_1}{dy}(K^{*0}) - \frac{dv_1}{dy}(K^+)$ and $\frac{dv_1}{dy}(\phi) - \frac{dv_1}{dy}(K^+)$ having opposite signs with the effect being more pronounced in central collisions as compared to peripheral ones due to the larger multiplicity as well as longer duration of the hadronic phase. Further, this effect is enhanced in low-energy collisions owing to a stronger breaking of boost invariance. On the contrary, the influence of the hadronic phase on the K^{*0} elliptic flow v_2 is found to be less significant and quantitative.

DOI: 10.1103/PhysRevC.109.044905

I. INTRODUCTION

The effect of the late-stage hadronic rescattering phase on the yield of resonances has been well studied. Short-lived resonances, like $\rho^0(770)$, $K^{*0}(892)$, $\Lambda^{*0}(1520)$, etc., decay within the hadronic medium formed in the late stage of relativistic heavy-ion collisions [1–6]. The resultant daughter particles undergo rescattering with other hadrons in the medium which inhibits the reconstruction of the resonace signal in experimental analysis [1–9]. This results in a notable reduction in the final yield of these resonances. On the other hand, pseudoinelastic interaction between the hadrons in the medium can increase the resonance yield through the regeneration process [9]. These hadronic state effects on resonances are experimentally verified by measuring the nonresonance to resonance yield ratio across systems of varying sizes [1,3–5,10,11]. The change in the yield of resonances depends on both the hadronic phase lifetime and the density of hadrons in the medium [12–17]. This distinctive behavior positions the resonances as ideal candidates for probing the hadronic phase of heavy-ion collisions.

The K^{*0} resonance has a short lifetime of ~ 4 fm/c. It decays to π and K in the medium. The resultant daughter pions mainly undergo scattering with the hadronic medium of the fireball that is dominantly pions leading to loss of signal of K^{*0}. However, the regeneration of K^{*0} is less pronounced due to the fact that the π-K cross section is smaller than that of π-π interactions [4,18–20]. Consequently, this gives rise to a reduction in the K^{*0} to K yield ratio in larger systems compared to $p+p$ collisions at equivalent collision energies. This distinguishing characteristic of the K^{*0} is used to get a rough estimate of the time span between chemical and kinetic freeze-outs in a given system [21,22]. Such in-medium effects can also influence the phase-space distribution of the K^{*0} resonance, which can in turn be reflected in the flow coefficients. The flow coefficients are characterized by different order harmonics in the Fourier series expansion of the azimuthal distribution of particles produced in momentum space:

$$\frac{dN}{p_T dp_T dy d\phi} = \frac{dN}{p_T dp_T dy}\left(1 + 2\sum_{n=0}^{\infty} v_n(p_T, y)\cos\left[n(\phi - \psi_n)\right]\right). \quad (1)$$

Here, ψ_n is the event plane angle associated with the nth-order harmonics. The variables p_T, y, and ϕ represent the transverse momentum, rapidity, and azimuthal angle of the produced particles, respectively.

It is known from earlier studies that the hadronic interactions affect the elliptic flow (v_2) of K^{*0} at low p_T [12]. In the current study, we focus on the rapidity-odd directed flow (v_1) of K^{*0}. The study of the v_1 of various light flavor hadrons has been conducted to provide deeper understanding of several key aspects. These include constraining the initial three-dimensional distribution of energy and baryon density in the medium [23–30], investigating the characteristics of the QCD equation of state [31,31–35], and extracting the transport coefficients of the medium [27,36–38]. The study of the v_1 of the K^{*0} resonance can provide information about the extent to which these resonances participate in the collective expansion of the system. Also, the impact of the hadronic afterburner on v_1 can yield insights into the coordinate as

*tribhu.451@gmail.com
†sandeep@iiserbpr.ac.in
‡nasim@iiserbpr.ac.in

well as the momentum space configuration of the late stage hadronic fireball.

In the next section we describe the framework that has been used in this study. The results are presented and explained in Sec. III and we summarize the findings in Sec. IV.

II. FRAMEWORK

The framework used in this study includes multiple components to simulate different stages of the heavy-ion collisions. A Glauber-based model has been used to set up the initial condition for the hydrodynamic evolution. The expansion of the resulting fireball is simulated by the publicly available MUSIC code [39–42]. The ISS code [43,44] has been used to sample the primordial hadrons from the hypersurface of constant energy density, generated from the space-time evolution of the fluid. Subsequently, the ultrarelativistic quantum molecular dynamics (UrQMD) code [20,45] is employed to simulate the interaction and expansion of the hadrons during the dilute phase of the heavy-ion collision.

Smooth transverse profiles of participant and binary collision densities have been prepared by averaging over 25 000 Monte Carlo (MC) Glauber events [26]. We have set the impact parameter direction along the x axis in each event. The participant and binary collision sources obtained from each MC Glauber event are rotated by the second-order participant plane angle and then smeared out in the transverse plane. The smearing profile is assumed to be a Gaussian with parametric width $\sigma_\perp = 0.4$ fm. Using the transverse profiles of participant and binary collision densities, we have constructed the initial profile of energy density at a constant proper time (τ_0) which takes the following form:

$$\epsilon(x, y, \eta_s; \tau_0) = \epsilon_0\{[N_+(x, y)f_+(\eta_s) + N_-(x, y)f_-(\eta_s)] \times (1 - \alpha) + N_{\rm bin}(x, y)\epsilon_{\eta_s}(\eta_s)\alpha\}, \quad (2)$$

where $N_+(x, y)$ and $N_-(x, y)$ are the participant densities of the nuclei moving with positive and negative rapidity, respectively. $N_{\rm bin}(x, y)$ accounts for the contributions from binary collision sources at each point in the transverse plane. α is the hardness factor which controls the relative contribution of participant and binary sources in the total deposited energy. The space-time rapidity (η_s) extension profile, $\epsilon_{\eta_s}(\eta_s)$, is an even function of η_s which has the following form:

$$\epsilon_{\eta_s}(\eta_s) = \exp\left(-\frac{(|\eta_s| - \eta_0)^2}{2\sigma_\eta^2}\theta(|\eta_s| - \eta_0)\right). \quad (3)$$

Here, η_0 and σ_η are two free parameters which are tuned to capture the rapidity differential charged-particle yield.

The functions $f_{+,-}(\eta_s)$ introduce the asymmetric deposition of matter in forward and backward rapidity regions:

$$f_{+,-}(\eta_s) = \epsilon_{\eta_s}(\eta_s)\epsilon_{F,B}(\eta_s), \quad (4)$$

with

$$\epsilon_F(\eta_s) = \begin{cases} 0, & \text{if } \eta_s < -\eta_m, \\ \frac{\eta_s + \eta_m}{2\eta_m}, & \text{if } -\eta_m \leqslant \eta_s \leqslant \eta_m, \\ 1, & \text{if } \eta_m < \eta_s, \end{cases} \quad (5)$$

and

$$\epsilon_B(\eta_s) = \epsilon_F(-\eta_s). \quad (6)$$

This deposition scheme creates a tilted profile of energy density in the reaction plane (the plane made by the impact parameter and beam direction of the collision) [23] where the tilt is controlled by the model parameter η_m.

The baryon deposition scheme used in this work was first introduced in Ref. [27], where the initial baryon distribution depends on both participant and binary collision sources. The three-dimensional distribution of the baryon density at τ_0 is

$$n_B(x, y, \eta_s; \tau_0) = N_B[W_+^B(x, y)f_+^B(\eta_s) + W_-^B(x, y)f_-^B(\eta_s)]. \quad (7)$$

$f_\pm^{n_B}$ are the rapidity envelope profiles for the net baryon deposition which are taken as [26,42]

$$f_+^{n_B}(\eta_s) = \left[\theta\left(\eta_s - \eta_0^{n_B}\right)\exp - \frac{\left(\eta_s - \eta_0^{n_B}\right)^2}{2\sigma_{B,+}^2} + \theta\left(\eta_0^{n_B} - \eta_s\right)\exp - \frac{\left(\eta_s - \eta_0^{n_B}\right)^2}{2\sigma_{B,-}^2}\right] \quad (8)$$

and

$$f_-^{n_B}(\eta_s) = \left[\theta\left(\eta_s + \eta_0^{n_B}\right)\exp - \frac{\left(\eta_s + \eta_0^{n_B}\right)^2}{2\sigma_{B,-}^2} + \theta\left(-\eta_s - \eta_0^{n_B}\right)\exp - \frac{\left(\eta_s + \eta_0^{n_B}\right)^2}{2\sigma_{B,+}^2}\right]. \quad (9)$$

Here, $\eta_0^{n_B}$ and $\sigma_{B,\pm}$ are the model parameters which are tuned to capture the rapidity differential net proton yield. $W_\pm^B(x, y)$ are the weight factors to deposit the net baryon in the transverse plane which have the following form:

$$W_\pm^B(x, y) = (1 - \omega)N_\pm(x, y) + \omega N_{\rm bin}(x, y). \quad (10)$$

The N_B in Eq. (7) is fixed by the constraint,

$$\int \tau_0 dx dy d\eta_s n_B(x, y, \eta_s; \tau_0) = N_{\rm part}, \quad (11)$$

where $N_{\rm part} = \int dxdy[N_+(x, y) + N_-(x, y)]$. The model parameter ω in Eq. (10) determines the proportionate contributions from participant and binary sources in the baryon profile. It has been observed that ω acts as a tilt parameter for the baryon profile [27]. The values of η_m and ω decide the relative tilt between the energy and the baryon density profile, and a suitable choice of the values of these two parameters can describe the experimentally measured $v_1(y)$ of $\pi^\pm$, p, $\bar{p}$ and other hadrons simultaneously [28].

We start the hydrodynamic evolution of the energy and the baryon density with zero initial transverse velocity by following the Bjorken flow ansatz. A constant specific shear viscosity ($C_\eta = \frac{\eta T}{\epsilon + p} = 0.08$) has been taken during the fluid evolution at all collision energies. However, we have not considered the effect of setting the bulk viscosity value to 0. To introduce nonzero baryon diffusion, we utilize the following expression for the baryon transport coefficient (κ_B) which is derived from the Boltzmann equation in the relaxation time

approximation [42]:

$$\kappa_B = \frac{C_B}{T} n_B \left[\frac{1}{3} \coth\left(\frac{\mu_B}{T}\right) - \frac{n_B T}{\epsilon + p} \right]. \tag{12}$$

In this equation, C_B is a model parameter governing the strength of baryon diffusion in the medium which we have taken as unity. In this expression, n_B represents the net baryon density, p is the local pressure, T corresponds to the temperature, and μ_B stands for the baryon chemical potential of the fluid. The equation of state (EoS) utilized in this study enforces both strangeness neutrality and a fixed baryon-to-charge density ratio within each fluid cell [46]. The particlization has been performed on the hypersurface characterized by the constant energy density ($\epsilon_f = 0.26$ GeV/fm^3) using the ISS code [43,44]. From the hypersurface, we have generated a large number of particlization events and in each event the resultant hadrons are subsequently put into UrQMD [20,45] for late-stage hadronic interactions.

The values of the model parameters taken in this study at different $\sqrt{s_{NN}}$ are the same as those taken in Ref. [28]. Notably, the model captures the experimental data of pseudorapidity differential charged-particle yield, p_T spectra of identified hadrons, p_T-dependent v_2 of charged hadrons, rapidity differential net proton yield and rapidity differential directed flow of identified hadrons with the chosen model parameters [27,28].

III. RESULTS

First, we have studied the directed flow of K^{*0} and ϕ in Au+Au collisions of 10–40% centrality at $\sqrt{s_{\rm NN}} = 27$ GeV. In order to investigate the effect of late-stage hadronic interaction, we have considered two different scenarios of final particle production. In the first scenario, primordial resonances produced from the hypersurface instantaneously decay into stable hadrons without undergoing any further interactions. In contrast, the second scenario involves feeding the primordial hadrons into UrQMD. Subsequently, the system of hadrons evolves through a sequence of binary collisions following the Boltzmann equation. In this latter case, the hadrons undergo multiple instances of both elastic and inelastic scattering in the hadronic phase to give the ultimate stable hadrons. Furthermore, the directed flow of primordial hadrons is also presented to demonstrate the exclusive effect of resonance decay on directed flow.

The rapidity-dependent directed flows of ϕ and K^{*0} are plotted in Figs. 1(a) and 1(b), respectively. Due to the small scattering cross sections, the phase-space distribution of the ϕ meson is less affected within the hadronic medium [47–49]. Further, owing to a larger lifetime than the fireball lifetime, ϕ is not affected by rescattering effects. Consequently, the v_1 of ϕ remains largely unaltered even after traversing through hadronic transport. However, the impact of hadronic transport is notably pronounced in K^{*0}. Remarkably, it is observed that the midrapidity slope of $v_1(y)$ for K^{*0} changes sign from negative (prior to the hadronic interaction) to positive (after the hadronic interaction).

To understand the underlying reason behind the significant alteration in the v_1 of K^{*0} during the hadronic phase, we have

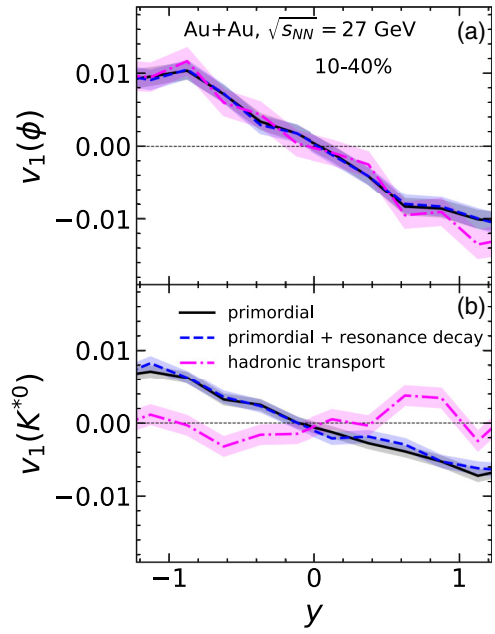

FIG. 1. The rapidity differential directed flow (v_1) of ϕ and K^{*0} has been plotted in panels (a) and (b), respectively, for Au+Au collisons of 10–40% centrality at $\sqrt{s_{NN}} = 27$ GeV. The v_1 of the primordial hadrons which are produced directly from the hypersurface is represented by solid lines. The dashed lines represent the v_1 calculations of the hadrons after performing the decay of resonances to stable hadrons, whereas the dashed-dotted lines represent the v_1 calculations of the hadrons after they pass through the UrQMD hadronic afterburner. The band in each line provides the statistical uncertainty in the calculation.

studied the variations in yield and v_1 for K^{*0} within distinct regions of its phase space. Our focus remained exclusive to the positive rapidity region ($0 < y < 1$), where we independently examined the behavior of hadrons flowing with $p_x > 0$ and $p_x < 0$. The ratio of integrated yield (N) and v_1 between hadrons with $p_x > 0$ and $p_x < 0$ is calculated as follows:

$$\frac{N_{(p_x>0)}}{N_{(p_x<0)}} = \frac{\int_0^1 dy \int_{-\pi/2}^{\pi/2} d\phi \int dp_T \frac{dN}{dp_T dy d\phi}}{\int_0^1 dy \int_{\pi/2}^{3\pi/2} d\phi \int dp_T \frac{dN}{dp_T dy d\phi}}, \tag{13}$$

$$\frac{(v_1)_{(p_x>0)}}{(v_1)_{(p_x<0)}} = \frac{\int_0^1 dy \int_{-\pi/2}^{\pi/2} d\phi \cos\phi \int dp_T \frac{dN}{dp_T dy d\phi}}{\int_0^1 dy \int_{\pi/2}^{3\pi/2} d\phi \cos\phi \int dp_T \frac{dN}{dp_T dy d\phi}} \times \frac{N_{(p_x<0)}}{N_{(p_x>0)}}. \tag{14}$$

We follow the same convention in setting up the coordinate system as is done in experiments to measure the rapidity-odd directed flow with respect to the first-order spectator plane [50–52]. As per this convention, the direction of deflection in the transverse plane to the beam axis of the spectators moving along the positive rapidity direction is labeled as the positive x axis. In our model calculations with a smooth Glauber initial condition, the positive x direction is given by the direction of the impact parameter vector drawn in the transverse plane to the beam axis from the center of the target nucleus (moving in the negative rapidity direction) to that of the projectile nucleus (moving in the positive rapidity direction) [23,27,28,53].

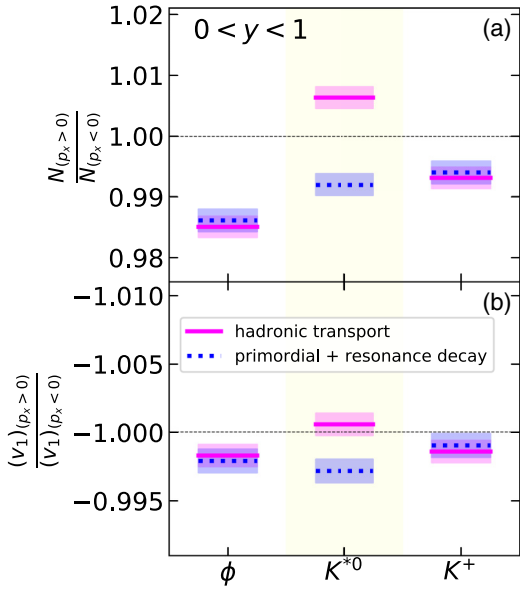

FIG. 2. The rapidity-integrated yield (a) and v_1 (b) ratios between hadrons of $p_x > 0$ and $p_x < 0$ [see Eqs. (13) and (14)] in Au+Au collisons of 10–40% centrality at $\sqrt{s_{NN}} = 27$ GeV. The rapidity integration has been performed between $0 < y < 1$. The ratios have been shown for ϕ, K^{*0}, and K^+. To show the results obtained under different conditions, specifically, with or without the inclusion of hadronic transport stages for the hadrons, we have plotted the ratios for scenarios involving solely primordial hadrons and their resonance decay contributions (dotted lines), as well as for cases where the hadrons undergo interactions in the hadronic medium (solid lines).

The comparison of the rapidity-integrated yield and v_1 ratios between hadrons with positive and negative p_x for ϕ, K^{*0}, and K^+ is depicted in Figs. 2(a) and 2(b), respectively. Within the plot, we present a comparison of outcomes obtained with and without the inclusion of hadronic transport stages for the hadrons.

It has been observed that the ratio of integrated yield for K^+ between $p_x > 0$ and $p_x < 0$ is less than 1, and this value changes a little during the hadronic interactions. Similarly, the ratio of the magnitude of average directed flow (v_1) also shows a minute change in the hadronic phase and continues to be less than 1. The same events sampled from the hypersurface are passed into UrQMD for late-stage hadronic transport. As a result, the error bars in both the yield ratio and the v_1 ratio between pre- and posthadronic stage effects are correlated. Therefore, the small deviations in the mean values of the ratios reflect the influence of the hadronic afterburner. This implies that more K^+ particles are produced with negative p_x, leading to the observed negative value of v_1 in the positive rapidity region, which remains unaltered throughout the late-stage evolution. The results are similar for ϕ as it mostly decays outside the fireball owing to a larger lifetime and hence there is a minimal rescattering effect from the afterburner. However, a significant effect of the hadronic afterburner has been noted in the ratio of integrated K^{*0} yield between particles with $p_x > 0$ and $p_x < 0$. After the hadronic interactions, the ratio $N_{(p_x>0)}/N_{(p_x<0)}$ becomes greater than 1, which contrasts the scenario where it was initially less than 1 in the absence of hadronic interactions. This change in the integrated yield ratio during the hadronic phase can be attributed to the distinct hadronic interactions experienced by K^{*0} particles in different regions of momentum space due to the initial tilted condition resulting in an asymmetric distribution of the hadronic fireball in both coordinate and momentum space.

Due to its short lifetime, the K^{*0} resonance decays into daughter particles (π and K) within the hadronic medium. If any of the daughter particles undergo a change in momentum due to interactions with other particles in the medium, it becomes unfeasible to reconstruct K^{*0} using this rescattered daughter particle. This phenomenon is referred to as the "signal loss" of the K^{*0} resonance [4,8,22,54–56]. In Fig. 2(a), we observe a higher signal loss for K^{*0} with $p_x < 0$, which gives rise to $N_{(p_x>0)}/N_{(p_x<0)} > 1$. The asymmetric signal loss on different sides of $p_x = 0$ stems from the unequal distribution of pions on the two sides of the beam axis in the reaction plane. The initial tilted profile leads to an asymmetric evolution of the fireball, whereby a predominantly large number of pions flow with negative p_x [23,25,57] resulting in an asymmetric distribution of the bath in coordinate space. As a result, K^{*0} particles with $p_x < 0$ located in the positive rapidity regions encounter a relatively denser pion medium. Consequently, a comparatively higher amount of rescattering occurs, contributing to a greater loss of K^{*0} signal in this region. Since we are capable of reconstructing more hadrons with $p_x > 0$, we obtain a v_1 that is more weighted by K^{*0} with $p_x > 0$. This leads to an overall positive v_1 for K^{*0} in the positive rapidity region. Due to the symmetry of the collision, the same mechanism makes the v_1 value of K^{*0} negative in the negative rapidity region.

The p_T-dependent v_1 values for both ϕ and K^{*0} are presented in Figs. 3(a) and 3(b), respectively. This p_T differential calculation has been done for particles produced in positive rapidity (y) within range $0 < y < 1$. The afterburner has a negligible effect on the v_1 of ϕ as expected. However, in the case of K^{*0}, a pronounced influence of hadronic interactions becomes evident, particularly at low p_T. The v_1 values of K^{*0} resonance at a relatively larger p_T region ($p_T > 1.5$ GeV/c) is already positive at the hadronization surface which indicates they are on the less dense side of the fireball and hence their decay products are likely to rescatter less, resulting in a reduced effect on the v_1. Further, they are more likely to decay outside the fireball and hence the daughters escape rescattering by the hadronic medium, allowing for reconstruction of K^{*0}.

The effect of hadronic interaction on the resonances is also reflected in the elliptic flow [12]. In Fig. 4, we have plotted the v_2 as a function of p_T for ϕ and K^{*0} resonances generated within the midrapidity $| y | < 0.5$ region. Notably, it has been observed that the elliptic flow magnitude of K^{*0} decreases for $p_T < 1.5$ GeV/c as there is likely to be larger K^{*0} loss along the in-plane direction than out of the reaction plane direction [54]. However, this suppression reduces as one goes to higher p_T consistent with the observations in the v_1 case. Conversely, the impact of hadronic transport on the v_2 of ϕ is minimal.

Our observation highlights a significant difference in the impact of hadronic interactions on the v_1 of ϕ and K^{*0}

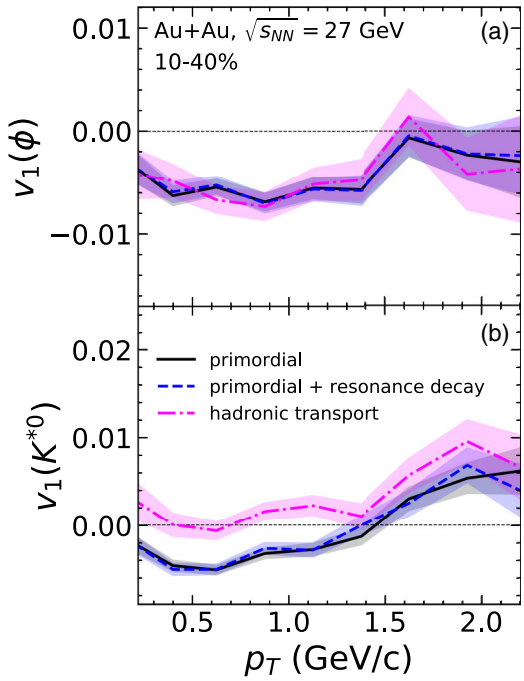

FIG. 3. The p_T differential directed flow (v_1) has been plotted for ϕ (a) and K^{*0} (b) for Au+Au collisons of 10–40% centrality at $\sqrt{s_{NN}} = 27$ GeV. The calculation has been done for the particles produced within the rapidity range $0 < y < 1$. The v_1 of the primordial hadrons which are produced directly from the hypersurface is represented by solid lines. The dashed lines represent the v_1 calculations of the hadrons after performing the decay of resonances to stable hadrons, whereas the dashed-dotted lines represents the v_1 calculations of the hadrons after they pass through the UrQMD hadronic afterburner.

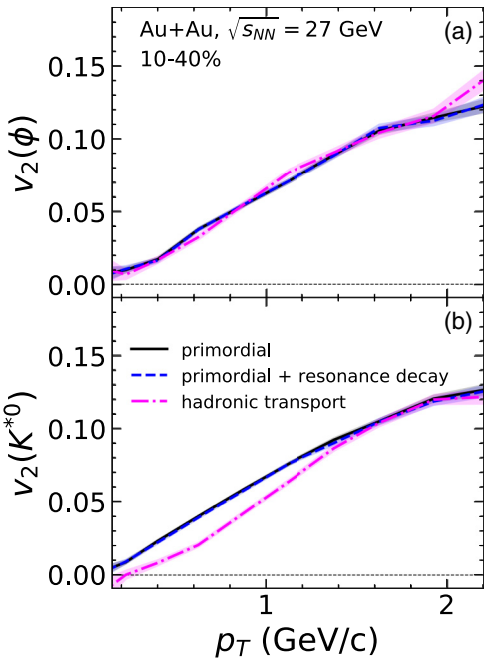

FIG. 4. Same as in Fig. 3 but for the p_T differential elliptic flow (v_2) of the hadrons produced within the rapidity range $|y| < 0.5$.

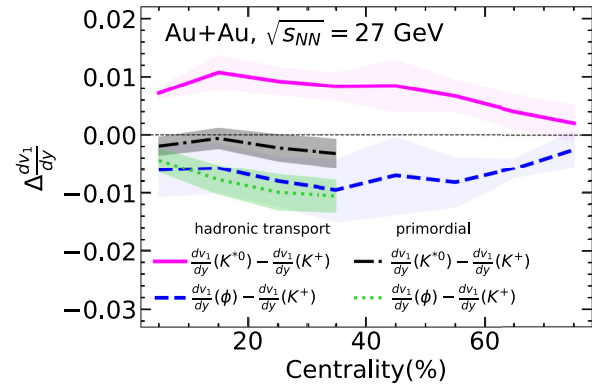

FIG. 5. The splitting of directed flow slopes ($\frac{dv_1}{dy}$) of resonances ϕ and K^{*0} with K^+ has been plotted as a function of centrality for Au+Au collisions at $\sqrt{s_{NN}} = 27$ GeV. The shaded bands denote the statistical uncertainties in the model calculations.

particles. This difference becomes particularly interesting when we study their dependence on centralities and collision energies. Such an investigation could provide deeper insights into the role played by the hadronic phase in heavy-ion collisions. While the absolute magnitude and sign of the v_1 slope of K^{*0} and ϕ may vary with centrality and $\sqrt{s_{NN}}$, but the relative dv_1/dy between K^{*0} and K, or between ϕ and K, will consistently reflect the exclusive influence of hadronic interactions on these resonances. In this regard, we present the centrality dependence of midrapidity v_1-slope splitting ($\Delta\frac{dv_1}{dy}$) between K^{*0} and K^+ in Au+Au collisons at $\sqrt{s_{NN}} = 27$ GeV in Fig. 5. Notably, the magnitude of splitting is least in peripheral collisions and gradually increases towards the central collisions. In peripheral collisions, the duration of the hadronic phase lifetime is relatively shorter, alongside a reduced production of pions. Consequently, this leads to a lesser afterburner effect in the hadronic phase. Conversely, in central collisions, the hadronic phase persists for a more extended period, thus allowing a more pronounced hadronic afterburner influence.

We have further examined the centrality trend of the midrapidity $\frac{dv_1}{dy}$ splitting between ϕ meson and K^+ in Fig. 5. This investigation is particularly more illuminating as the v_1 of ϕ and K^+ appears to be less influenced by hadronic scatterings. Our findings reveal that $[\frac{dv_1}{dy}(\phi) - \frac{dv_1}{dy}(K^+)]$ consistently maintains a negative value across all centralities. This suggests that $|\frac{dv_1}{dy}(\phi)| > |\frac{dv_1}{dy}(K^+)|$ holds true for all centralities, which is an anticipated outcome stemming from the mass hierarchy. For comparison, we also depict $[\frac{dv_1}{dy}(K^{*0}) - \frac{dv_1}{dy}(K^+)]$ for primordial hadrons, showing a consistently negative sign following the mass hierarchy. Interestingly, the sign of $[\frac{dv_1}{dy}(K^{*0}) - \frac{dv_1}{dy}(K^+)]$ shifts to positive after the hadronic transport stage at all centralities. This is a clear signature of the hadronic stage effect on the K^{*0} resonance which could be measured in experiments.

The collision energy dependence of the splitting of the directed flow slope between K^{*0} and K^+ has been plotted in Fig. 6 for Au+Au collisions of 10–40% centrality. It has been observed that the splitting is less in higher $\sqrt{s_{NN}}$ and it

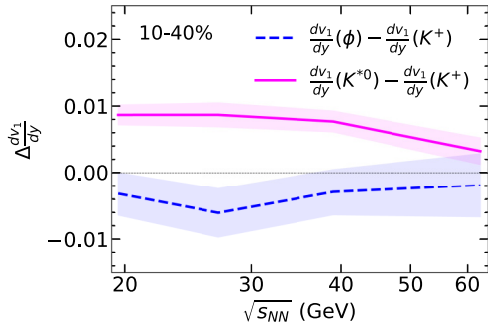

FIG. 6. The splitting of directed flow slopes ($\frac{dv_1}{dy}$) between K^{*0} and K^+, along with ϕ and K^+, has been plotted as a function of the collision energy ($\sqrt{s_{NN}}$) for Au+Au collisions of 10–40% centrality.

becomes more pronounced at lower collision energies owing to the larger tilt of the fireball at lower energies resulting in a larger asymmetric hadronic fireball at lower energies affecting the v_1 of K^{*0} more strongly. For comparison, we have also plotted the splitting between ϕ and K^+ that remains constant at ~ -0.005. Note that at even lower energies baryon stopping physics give rise to nontrivial dynamics of conserved charges that could affect the directed flow of these resonances, particularly that of K^{*0} as it carries strangeness.

IV. SUMMARY

In this work we have studied the effect of late-stage hadronic interaction on the rapidity-dependent directed flow (v_1) of K^{*0} in a hybrid (hydrodynamics+hadronic transport) framework. The study compares the v_1 results calculated from the hadrons which are directly produced from the hypersurface and resonance decay with those that undergo hadronic transport. The analysis reveals that the v_1 of K^{*0} is strongly affected during the hadronic stage due to asymmetric signal loss in different sides of the p_x axis in momentum space caused by the tilted fireball. We have also analyzed the flow of ϕ for reference. We find that owing to a small cross section and a long lifetime, the flow of ϕ is unaffected by the hadronic afterburner.

The centrality dependence of the effect of hadronic interaction on the v_1 of K^{*0} has been studied by plotting the splitting of v_1 between K^+ and K^{*0} as a function of centrality at $\sqrt{s_{NN}} = 27$ GeV. Notably, the observed splitting is minimal in peripheral collisions and progressively increases as collisions become more central. This trend signifies that the impact of hadronic interactions is most significant in central collisions, which can be attributed to the relatively longer duration of the hadronic phase and the comparatively higher yield of produced hadrons. Furthermore, the beam energy dependence of the v_1 splitting between K^+ and K^{*0} has been studied within the 10–40% centrality range. Interestingly, the effect of hadronic interactions becomes more pronounced in collisions with lower energy. This can be attributed to the larger tilt in the initial fireball, resulting in an increasingly asymmetric distribution of the hadronic medium in coordinate and momentum space. In our model calculation, we have utilized a smooth initial condition that effectively captures the tilted geometry of the fireball. However, it is important to note that event-by-event fluctuations in the initial state would affect the spatial asymmetry of the initial fireball and consequently influence the final-state flow observables. While the generation of v_1 and asymmetric signal loss is primarily a consequence of geometry, there still exists a finite but less significant effect due to fluctuations. Therefore, the nature of the results presented in this paper is qualitative. We also emphasize that, for a more quantitative prediction or model-to-data comparison, simulations should be conducted with a fluctuating initial condition. Moreover, a comprehensive and quantitative investigation of the flow coefficients associated with K^{*0} and other resonances, along with the model to experimental data comparison, holds the potential of yielding deeper insights into the nature of the hadronic phase.

[1] S. Acharya *et al.* (ALICE Collaboration), Phys. Rev. C **99**, 024905 (2019).
[2] S. Acharya *et al.* (ALICE Collaboration), Eur. Phys. J. C **80**, 160 (2020).
[3] S. Acharya *et al.* (ALICE Collaboration), Phys. Rev. C **99**, 064901 (2019).
[4] J. Adams *et al.* (STAR Collaboration), Phys. Rev. C **71**, 064902 (2005).
[5] B. B. Abelev *et al.* (ALICE Collaboration), Phys. Rev. C **91**, 024609 (2015).
[6] J. Song (ALICE Collaboration), Nucl. Phys. A **967**, 920 (2017).
[7] S. Acharya *et al.* (ALICE Collaboration), Phys. Lett. B **802**, 135225 (2020).
[8] M. M. Aggarwal *et al.* (STAR Collaboration), Phys. Rev. C **84**, 034909 (2011).
[9] M. Bleicher and J. Aichelin, Phys. Lett. B **530**, 81 (2002).
[10] B. I. Abelev *et al.* (STAR Collaboration), Phys. Rev. Lett. **97**, 132301 (2006).
[11] D. Adamova *et al.* (ALICE Collaboration), Eur. Phys. J. C **77**, 389 (2017).
[12] D. Oliinychenko and C. Shen, arXiv:2105.07539.
[13] S. Cho and S. H. Lee, Phys. Rev. C **97**, 034908 (2018).
[14] A. K. Sahoo, M. Nasim, and S. Singha, Phys. Rev. C **108**, 044904 (2023).
[15] C. Le Roux, F. S. Navarra, and L. M. Abreu, Phys. Lett. B **817**, 136284 (2021).
[16] K. Werner, A. G. Knospe, C. Markert, B. Guiot, I. Karpenko, T. Pierog, G. Sophys, M. Stefaniak, M. Bleicher, and J. Steinheimer, EPJ Web Conf. **171**, 09002 (2018).
[17] A. G. Knospe, C. Markert, K. Werner, J. Steinheimer, and M. Bleicher, Phys. Rev. C **104**, 054907 (2021).
[18] S. D. Protopopescu, M. Alston-Garnjost, A. Barbaro-Galtieri, S. M. Flatte, J. H. Friedman, T. A. Lasinski, G. R. Lynch,

M. S. Rabin, and F. T. Solmitz, Phys. Rev. D **7**, 1279 (1973).
[19] M. J. Matison, A. Barbaro-Galtieri, M. Alston-Garnjost, S. M. Flatte, J. H. Friedman, G. R. Lynch, M. S. Rabin, and F. T. Solmitz, Phys. Rev. D **9**, 1872 (1974).
[20] M. Bleicher *et al.*, J. Phys. G: Nucl. Part. Phys. **25**, 1859 (1999).
[21] A. Motornenko, V. Vovchenko, C. Greiner, and H. Stoecker, Phys. Rev. C **102**, 024909 (2020).
[22] M. Abdallah *et al.* (STAR Collaboration), Phys. Rev. C **107**, 034907 (2023).
[23] P. Bozek and I. Wyskiel, Phys. Rev. C **81**, 054902 (2010).
[24] S. Ryu, V. Jupic, and C. Shen, Phys. Rev. C **104**, 054908 (2021).
[25] Z.-F. Jiang, S. Cao, X.-Y. Wu, C. B. Yang, and B.-W. Zhang, Phys. Rev. C **105**, 034901 (2022).
[26] C. Shen and S. Alzhrani, Phys. Rev. C **102**, 014909 (2020).
[27] T. Parida and S. Chatterjee, arXiv:2211.15729.
[28] T. Parida and S. Chatterjee, arXiv:2211.15659.
[29] P. Bozek, Phys. Rev. C **106**, L061901 (2022).
[30] Z.-F. Jiang, X.-Y. Wu, S. Cao, and B.-W. Zhang, Phys. Rev. C **107**, 034904 (2023).
[31] J. Steinheimer, J. Auvinen, H. Petersen, M. Bleicher, and H. Stöcker, Phys. Rev. C **89**, 054913 (2014).
[32] D. H. Rischke, Y. Pürsün, J. A. Maruhn, H. Stoecker, and W. Greiner, Acta Phys. Hung. A **1**, 309 (1995).
[33] Y. Nara, H. Niemi, A. Ohnishi, and H. Stöcker, Phys. Rev. C **94**, 034906 (2016).
[34] Y. B. Ivanov and A. A. Soldatov, Eur. Phys. J. A **52**, 246 (2016).
[35] Y. B. Ivanov and A. A. Soldatov, Phys. Rev. C **91**, 024915 (2015).
[36] T. Parida and S. Chatterjee, arXiv:2305.10371.
[37] J. Mohs, M. Ege, H. Elfner, and M. Mayer (SMASH Collaboration), Phys. Rev. C **105**, 034906 (2022).
[38] F. Becattini, G. Inghirami, V. Rolando, A. Beraudo, L. Del Zanna, A. De Pace, M. Nardi, G. Pagliara, and V. Chandra, Eur. Phys. J. C **75**, 406 (2015); **78**, 354(E) (2018).
[39] B. Schenke, S. Jeon, and C. Gale, Phys. Rev. C **82**, 014903 (2010).
[40] B. Schenke, S. Jeon, and C. Gale, Phys. Rev. C **85**, 024901 (2012).
[41] J.-F. Paquet, C. Shen, G. S. Denicol, M. Luzum, B. Schenke, S. Jeon, and C. Gale, Phys. Rev. C **93**, 044906 (2016).
[42] G. S. Denicol, C. Gale, S. Jeon, A. Monnai, B. Schenke, and C. Shen, Phys. Rev. C **98**, 034916 (2018).
[43] C. Shen, Z. Qiu, H. Song, J. Bernhard, S. Bass, and U. Heinz, Comput. Phys. Commun. **199**, 61 (2016).
[44] The iSS code package can be downloaded from https://github.com/chunshen1987/iSS.
[45] S. A. Bass *et al.*, Prog. Part. Nucl. Phys. **41**, 255 (1998).
[46] A. Monnai, B. Schenke, and C. Shen, Phys. Rev. C **100**, 024907 (2019).
[47] T. Hirano, U. W. Heinz, D. Kharzeev, R. Lacey, and Y. Nara, Phys. Rev. C **77**, 044909 (2008).
[48] S. Takeuchi, K. Murase, T. Hirano, P. Huovinen, and Y. Nara, Phys. Rev. C **92**, 044907 (2015).
[49] A. Shor, Phys. Rev. Lett. **54**, 1122 (1985).
[50] B. I. Abelev *et al.* (STAR Collaboration), Phys. Rev. Lett. **101**, 252301 (2008).
[51] G. Agakishiev *et al.* (STAR Collaboration), Phys. Rev. C **85**, 014901 (2012).
[52] B. Abelev *et al.* (ALICE Collaboration), Phys. Rev. Lett. **111**, 232302 (2013).
[53] L. Du, C. Shen, S. Jeon, and C. Gale, Phys. Rev. C **108**, L041901 (2023).
[54] Z. Li, W. Zha, and Z. Tang, Phys. Rev. C **106**, 064908 (2022).
[55] B. Abelev *et al.* (ALICE Collaboration), Eur. Phys. J. C **72**, 2183 (2012).
[56] S. Acharya *et al.* (ALICE Collaboration), Phys. Lett. B **828**, 137013 (2022).
[57] J. Jing, Z.-F. Jiang, C. B. Yang, and B.-W. Zhang, Chin. Phys. C **47**, 034104 (2023).